Boletim da Sociedade Astronômica Brasileira, **34**, no. 1, 274-277

From Blue Cloud to Red Sequence: dissecting morphology and star formation variations across galaxies evolution

V. M. Sampaio,[1,2] R. R. de Carvalho ,[1] I. Ferreras,[3,4,5] A. Aragón-Salamanca,[2] L. C. Parker[6]

[1] NAT - Universidade Cruzeiro do Sul / Universidade Cidade de São Paulo, 01506-000, SP, Brazil e-mail: vitorms999@gmail.com
[2] School of Physics and Astronomy, University of Nottingham, University Park, Nottingham NG7 2RD, UK
[3] Instituto de Astrofísica de Canarias, Calle Vía Láctea s/n, E38205, La Laguna, Tenerife, Spain
[4] Department of Physics and Astronomy, University College London, Gower Street, London WC1E 6BT, UK
[5] Departamento de Astrofísica, Universidad de La Laguna, E38206 La Laguna, Tenerife, Spain
[6] Department of Physics and Astronomy, McMaster University, Hamilton ON L8S 4M1, Canada

Abstract. We investigate a sample of 254 clusters from the SDSS-DR7 Yang Catalog and an auxiliary sample of field galaxies to detail how star formation quenching in galaxies depends on both environment and galaxy stellar mass. Dissecting the star formation rate vs stellar mass diagram we provide evidence that galaxies rapidly change their morphology after reaching the green valley region, while there is still room for star formation rate decrease towards the red sequence. This provides a first suggestion that galaxies in clusters change their morphology prior to full star formation quenching. Moreover, we provide a first estimate on the time delay between morphological and specific star formation rate variation through the relation between location in the Projected Phase Space and infall time. We show that the transition from late to early-type morphology happens roughly in Δt_{inf} ∼1 Gyr, whereas the quenching of star formation takes ∼3 Gyr to be fully quenched. The time-scale we estimate for morphological transitions is similar to the expected for the delay phase in the delayed-then-rapid quenching model, for which we then suggest this phase as dominated by morphological transformations.

Resumo. Investigamos uma amostra de 254 aglomerados do Catálogo Yang do SDSS-DR7 e uma amostra auxiliar de galáxias de campo para detalhar como a extinção da formação de estrelas nas galáxias depende do ambiente e da massa estelar da galáxia. Dissecando o diagrama de taxa de formação de estrelas versus massa estelar, fornecemos evidências de que as galáxias mudam rapidamente sua morfologia depois de atingir a região do Green Valley, enquanto ainda há espaço para a diminuição da taxa de formação de estrelas em direção à Red Sequence. Isso fornece uma primeira sugestão de que as galáxias em aglomerados mudam sua morfologia antes da extinção completa da formação estelar. Além disso, fornecemos uma primeira estimativa sobre o intervalo de tempo entre a variação morfológica e da taxa de formação estelar específica através da relação entre a locus no Espaço de Fase Projetada e o infall time. Mostramos que a transição de Late para Early Type ocorre aproximadamente em um intervalo de Δt_{inf} ∼1 Gyr, enquanto a extinção da formação estelar leva ∼3 Gyr. A escala de tempo estimada para as transições morfológicas é semelhante à esperada para a fase de "delay" no modelo de extinção "slow-then-rapid", para o qual então sugerimos esta fase como dominada por transformações morfológicas.

Keywords. Galaxies: clusters: general – Galaxies: evolution – Galaxies: general

1. Introduction

Galaxies are divided according to their morphology into two major classes: Early Type (ETGs) – elliptical shapes – and Late Type Galaxies (LTGs) – combination of bulge and spiral arms. A bimodal distribution is also seen in galaxy stellar population properties, which then defines two major and one intermediate region regarding galaxy evolution: 1) Blue Cloud (BC) – filled mainly by blue, star forming LTGs; 2) Red Sequence (RS) – dominated by ETGs with low (if any) star formation; and 3) an intermediate region called the Green Valley (GV) – containing galaxies half-way to the full star formation quenching and with a wide range of morphologies (Schawinski et al. 2009; Masters et al. 2010a,b; Schawinski et al. 2014).

When a galaxy is isolated, star formation quenching is shown to rely mainly in internal properties. s (Larson 1974; Dekel & Silk 1986; Vulcani et al. 2021). For instance, outflows – usually generated by Active Galactic Nuclei feedback – can prevent gas accretion from the circumgalactic medium and remove the galaxy's gas reservoir (Dalla Vecchia & Schaye 2008; Bongiorno et al. 2016; Trussler et al. 2020). However, when galaxies experience high density environments, additional mechanisms come into play, which results in a complex and non-linear evolution. The most noteworthy is Ram Pressure Stripping – in which the hot gas in the intracluster medium (ICM) exerts pressure on galaxies moving within the cluster and may remove their gas component (Gunn & Gott 1972; Abadi et al. 1999, RPS). Moreover, it is important to highlight that clusters are built up by the accretion of galaxy groups, which means that infalling galaxies may have their properties altered even before entering the cluster environment – a phenomenon known as "pre-processing" (Fujita 2004; Mahajan 2013; Sarron et al. 2019).

The relation between galaxy properties and quenching mechanisms translates to a variety of paths for galaxy's transition from the BC to RS. In clusters, this is also expected to be a function of the time galaxies have been experiencing the high density environment – which is measured by the infall time . An ideal approach would be to use the well know galaxies' trajectories in the Phase Space to estimate their infall time (Rhee et al. 2017, see their Fig. 1). However, astronomers are limited by projected along the line of sight quantities, which causes a degeneracy in galaxies spatial distribution. To address that, a common technique is to use simulations and then study how the distribution of galaxies in the Phase Space translate to its projected version, the Projected Phase Space (Mahajan et al. (2011) and Oman et al. (2013)). Despite all the caveats, the PPS provide a power-

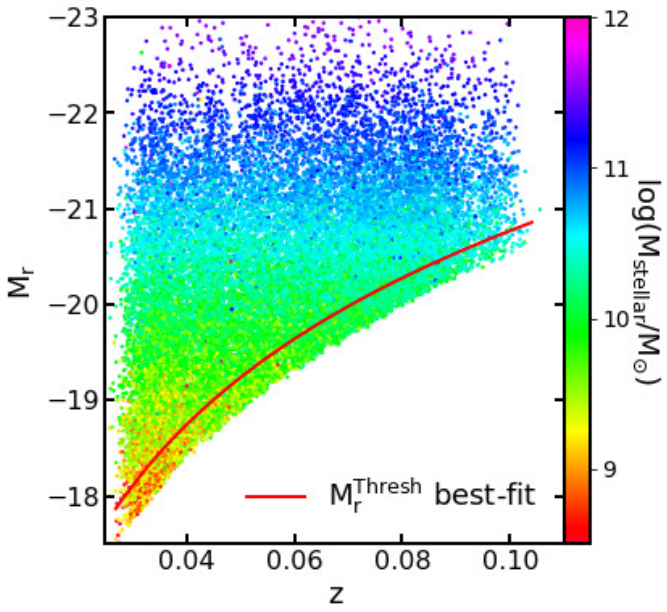

Figure 1. Relation between absolute magnitude and redshift for our full sample. Points are colored according to galaxy stellar mass. The red line denotes the 90% M_r threshold for each redshift.

ful tool to understand the effect of high density environments in galaxy evolution and their respective timescales (Ribeiro et al. 2013; Roberts & Parker 2017; de Carvalho et al. 2019; Sampaio et al. 2021).

In this work, we investigate the evolution of morphology and star formation rate as a function of galaxies evolutionary stage. We first address the question on whether SFR or morphology changes more quickly in cluster environments by using of the SFR vs $M_{stellar}$ plane to investigate their path from BC to RS as a function of stellar mass. Second, in particular to cluster, we investigate differents region in the Projected Phase Space (PPS) to derive a first estimate on the morphological transition timescale. Lastly, we investigate how variations in morphology and star formation rate depend on stellar mass and environment. Throughout this work we adopt a flat ΛCDM cosmology with $[\Omega_M, \Omega_\Lambda, H_0] = [0.27, 0.73, 72\ \mathrm{km\ s^{-1} Mpc^{-1}}]$.

2. Data selection and methods

In this work, we select galaxies from the SDSS-DR7 (Abazajian et al. 2007). Our sample the redshift range $0.03 \leq z \leq 0.1$ and Petrosian apparent magnitude in the r-band $m_r \leq 17.78$. Also available in the SDSS database, we select Stellar Mass ($M_{stellar}$, hereon) , SFR and sSFR from the MPA-JHU catalog (e.g. Brinchmann et al. 2004). To guarantee completeness, we only use galaxies above the 90th percentile in absolute magnitude. Fig. 1 shows the relation between absolute magnitude and redshift, with points colored according to galaxies stellar mass. The red solid line denotes the 90% M_r threshold for each redshift.

We further characterize galaxies' stellar population properties by selecting Age and Stellar Metallicity from the de Carvalho et al. 2017 (dC17, hereafter) catalog. Briefly, it uses the STARLIGHT code (Cid Fernandes et al. 2005) to perform a linear combination of predefined single stellar population (SSP) in order to get the best fit to the observed spectra. Since spectral fitting codes allow for an arbitrary weighting, we make use of the luminosity weighted derived age and [Z/H], such that the estimates are closely related to the last star formation episode (Trussler et al. 2020). Finally, we use the TType parameter to trace morphology, which was originally (de Vaucouleurs 1963) defined to classify lenticular galaxies (S0, T-Type = 0). We select TType from the Domínguez-Sánchez et al. (2018) catalog, which uses Convolutional Neural Network based Deep Learning Algorithms to provide morphological characterization of 670,722 galaxies from the SDSS database. We highlight that, differently from the original discrete TType definition, in this case it is measured as a real number, which is achieved by using the equation

$$\mathrm{T\,Type} = -4.6\,\mathrm{P(Ell)} - 2.4\,\mathrm{P(S0)} + 2.5\,\mathrm{P(Sab)} + 6.1\,\mathrm{P(Scd)} \quad (1)$$

where P denotes the probability attributed by the CNN to a given morphology. Moreover, special attention is given to the mixture between ETGs and S0s, which in their work is addressed by a focused model that achieves 86% precision (see their Fig. 13 for more details) in separating S0 and elliptical galaxies.

We assess galaxies' host environment via the Yang Group Catalog (Yang et al. 2007). Briefly, it provides a list of galaxies hosted by the same dark matter halo, which then allow us to define cluster and field samples. The former one is defined using an updated version of the Yang Group Catalog presented in dC17, which applies a "Shiftgapper" technique (see Fadda et al. 1996 for more details) to clusters listed with at least 20 members. This is important to the work proposed since it: 1) avoids prior assumptions about the cluster's dynamical stage; and 2) is more permissive regarding galaxies at larger distances from the cluster centre, which is relevant when considering the evolution of satellite galaxies in higher density environments.

Complementary, we define a control sample built with field galaxies in order to trace how galaxies evolve when in isolation. First, we select all galaxies with reliable spectroscopic redshift in the SDSS-DR7, with the same selection criteria of the cluster sample. We then use the following procedure to select field galaxies:

1. identify all groups from the Yang Catalog with $M_{Halo} \geq 10^{13} M_\odot$, which is a typical halo mass of poor groups ($N_{members} \leq 10$);
2. for each structure, estimate the virial radius using the scaling relation $R_{vir} \sim 1.61\,\mathrm{Mpc} \left(\frac{M_{halo}}{10^{14} M_\odot}\right)^{1/3} (1 + z_{group})^{-1}$;
3. select all galaxies classified as Isolated Central in the Yang Group Catalog and that lies beyond 5 R_{200} of every structure with halo mass greater than $10^{13} M_\odot$ listed in the same catalog;
4. consider galaxies only in the $[120 \leq RA \leq 250, 0 \leq DEC \leq 60]$ range, which consists of the main part of the SDSS footprint, such that edge effects are minimized.

This results in a set of 12,398 galaxies, that we hereafter use as our field sample.

3. Results

3.1. Dissecting the star formation rate vs. stellar mass plane to trace galaxy property variations

The discrete division of galaxies in BC, GV and RS is by itself incomplete due to the continuous nature of galaxy evolution. In order to better understand how galaxies evolve from the BC towards the RS, we create 17 different regions in the SFR vs

$M_{stellar}$ plane for the cluster sample. The limits of each region are defined as:

$$\log(SFR) = 0.7\log(M_{stellar}) - i \quad (2)$$

with i varying from 6.5 to 9.5 in steps of 0.17, which guarantees a minimum of $\sim$ 50 galaxies per slice. We present these regions as white dashed lines in Fig. 2. We then select galaxies within each slice and create normalized kernel density estimates for age, [Z/H] and TType. An important feature is the different number of galaxies in each slice. We then define a number-dependent bandwidth for the kernel density estimate, given as:

$$BW = 1.5 \times \frac{2 \times IQR}{N^{1/3}}, \quad (3)$$

where BW is the bandwidth, IQR is the interquartile range[1] and N is the number of points in the slice. Equation 3 is 1.5 times the optimal bin width of a histogram characterized by a given IQR and N. The factor 1.5 is empirically defined to slightly reduce the noise while preserving global trends. For each distribution, we trace the kernel peak density. However, as we adopt the normalized kernel, the peak density is directly related to the "width" of the observed distribution. Namely, high peaks denote narrower distributions, whereas low density values are related to broader distributions. We use a bootstrap technique with N=1000 repetitions to assess errorbars. We define the Star Formation Main Sequence (SFMS) as the slice containing the best linear fit of the BC galaxies. The inset in each panel shows variation of the Full Width Half Maximum (FWHM) in order to quantify the mixture of galaxy population properties in each slice.

This procedure results in a series of trends that are directly related galaxy evolution and, more importantly, to how cluter environment affect it. From all the trends, we highlight the found for GV distributions. In a few words, exploring the trends of galaxy properties across the the SFR vs $M_{stellar}$ plane we find that The GV denotes the region in which we find the transition towards broader and narrower age and [Z/H] distributions, respectively, and a significant TType peak variation from LTG to ETG morphology. It is noteworthy that galaxy morphology changes towards early-type shapes in just a few "slices", which suggests that most of the morphological transformation (if it happens) takes place in the green valley region. For a detail description please see Sampaio et al. (2022)

3.2. Estimating time-scales for morphological transition and star formation quenching

By exploring the Star Formation Rate vs. Stellar Mass plane, we find a first suggestion that morphological transition can happen prior to the full star formation quenching. Yet, our previous analysis does not take into account time in a direct way. In other words, the transition from one slice to the other can happen in different time intervals. Now we directly probe the time-scales related to morphological transition and star formation quenching for satellite galaxies infalling into cluster by the way of the Projected Phase Space. Furthermore, we use the relation between location in the Projected Phase Space and Infall Time as presented in Pasquali et al. (2018). With this relation, we trace the variations in morphology and specific star formation rate (= star formation rate / stellar mass) in the same infall time interval ($\sim$ 5Gyr). For each region defined in Pasquali et al.(2018), we calculate the median and 1-sigma error bars for T-Type and Specific Star Formation Rate. Since in both cases, we cover the same infall time interval, we can join this measurements in a single space, the T-Type vs. Specific Star Formation Rate space, which we can directly use to probe which parameter shows higher variation. The result is shown in Fig. 3.

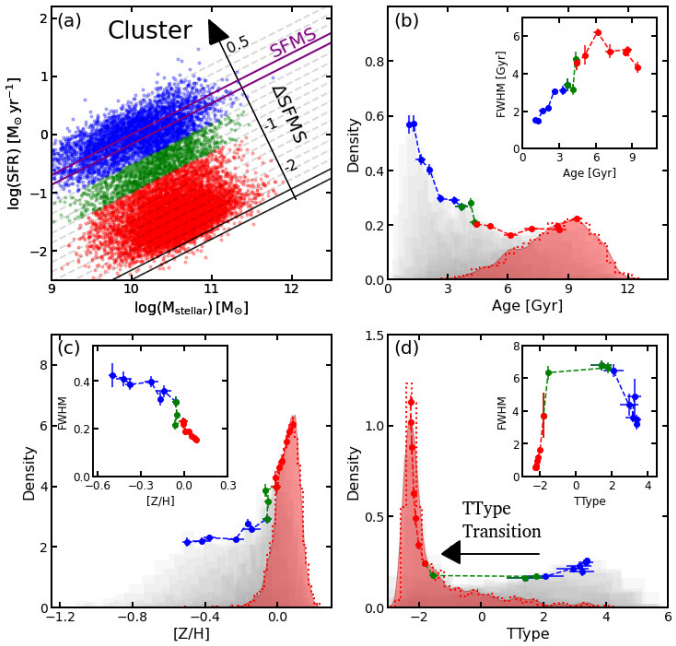

Figure 2. The image seen is the last frame/slice of the following procedure for cluster galaxies: 1) select galaxies within the solid black line slice highlighted in panel [a]; 2) build a probability density histogram for each property (Age, [Z/H] and TType). In this case, we use the Scott criteria (Scott 1979) to define the bin size in order to account for different number of points in each slice; 3) for each case we create a normalized epanechnikov kernel density estimate with bandwith set to 1.5 times the histogram bin; 4) we then estimate the peak density, FWHM and related errorbars using a bootstrap technique (with N = 1000 repetitions) for each slice. The curves in panels [b], [c] and [d] are the evolution of the peak density (large panel) and FWHM (miniature panel) as we progress from the top most slice to the bottom one. We color points and histograms according to the region in which the slice is (BC - blue, GV - green, RS - red). For completeness, as we evolve from top to bottom slice, we maintain the distributions from previous slices, which is shown as faded gray in each plot. The purple lines in panel [a] denote the slice containing the SFMS, which we then use the ΔSFMS to report our results. In the same panel, we also add an arrow indicating increasing ΔSFMS. Finally, in panel [d] we stress through a black arrow the significant TType transition experienced by galaxies during the GV. Due to the use of a normalized kernel, there is a relation between peak density and FWHM, namely increasing peak density means decreasing FWHM. See Sampaio et al. (2021b) for more details.

We find that more massive galaxies already enter the cluster as ETGs and then environmental effects (excluding mergers) do not cause significant variations in either TType or sSFR. Moreover, Fig. 3 results show unequivocally a higher variation in both TType and sSFR for less massive galaxies, strengthening the role of high density environments in driving low mass galaxies evolution. The pivotal result of our work is the especially rapid change we observe in galaxies' morphology. Quantitatively, in a $\Delta t_{inf} \sim$ 1 Gyr, low mass (cyan) galaxies experience a variation in TType (sSFR) corresponding to $\sim$ 60% ($\sim$

[1] Defined as the distance between the 75% and 25% quartiles.

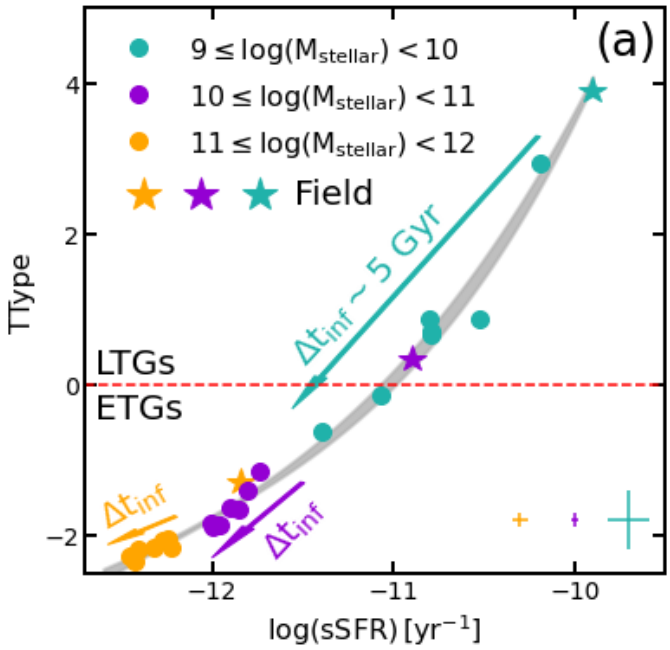

Figure 3. Relation between TType and sSFR for a fixed interval of time since infall (5 Gyr). Each point represents the median TType and sSFR for a single PNZ (and hence infall time) in the PPS. Galaxies are divided according to stellar mass (cyan, purple and orange). We present the mean errors in each case in the lower left corner. The colored arrows illustrate increasing infall time for each stellar mass bin. We add a spline fit and 1σ error as a grey dashed area. The median values of the field counterpart is displayed as the colored stars and the separation between LTGs and ETGs is denoted by the red dashed horizontal line.

28%) of the whole variation observed during the entire $\Delta t_{inf} \sim 5$ Gyr. Finally, it is noticeable that low mass galaxies reach the TType = 0 before being completely quenched. Therefore, our results provide strong evidence of a quicker morphological transition in comparison to star formation quenching.

4. Conclusion

After closely analysing the variation of galaxies properties during their transition from the Blue Cloud to Red Sequence in the Star Formation Rate vs. Stellar mass plane and quantifying timescales using the relation between locus in the projected phase space and infall time, we highlight the following conclusions:

1. Our analysis provides observational evidence of a considerable fraction of galaxies undergoing a transition from early to late-type morphologies in the Green Valley. Thus, we interpret this as a first evidence that galaxies in clusters change their morphology prior to the full quenching of star formation. Yet, it is important to stress that galaxy evolution is not linear and galaxies can reform a disk after a merger;
2. The relations between infall time and galaxy properties show the combined effect of environment and stellar mass driving galaxy evolution. Low mass galaxies are the most affected by environmental quenching mechanisms, whereas more massive systems rely mostly on internal mechanisms to halt their star formation;
3. We estimate that low mass galaxies infalling in clusters in the local universe suffer a rapid (~ 1 Gyr) morphological transition (LTG to ETG) just after crossing the virial radius for its very first time, while specific star formation keeps decreasing for a longer period of time (~ 3 Gyr);

Finally, we interpret that the delay between morphological transition and star formation quenching is directly related to the delay phase in the delayed-then-rapid quenching model for galaxies infalling in clusters. Namely, the similarity in the derived timescales suggest that this phase is mostly characterized by morphological transition, whereas star formation rate decreases at a slower rate. In the rapid phase, a combination of environmental effects (Ram Pressure Stripping, for example) further quench low mass galaxies by removing most of their gas content in a short time-scale (~ 1 - 3 Gyr).

Acknowledgements. VMS acknowledges the FAPESP scholarships through the grants 2020/16243-3 and 2021/13683-5. RdC aknowledges the financial support from FAPESP through the grant #2014/11156-4. IF acknowledges support from the Spanish Ministry of Science, Innovation and Universities (MCIU), through grant PID2019-104788GB-I00. LCP thanks the National Science and Engineering Research Council of Canada for funding.

References

de Carvalho R. R., Ribeiro A. L. B., Stalder D. H., Rosa R. R., Costa A. P., Moura T. C., 2017, AJ, 154, 96. doi:10.3847/1538-3881/aa7f2b
Cid Fernandes R., Mateus A., Sodré L., Stasińska G., Gomes J. M., 2005, MNRAS, 358, 363. doi:10.1111/j.1365-2966.2005.08752.x
Domínguez Sánchez H., Huertas-Company M., Bernardi M., Tuccillo D., Fischer J. L., 2018, MNRAS, 476, 3661. doi:10.1093/mnras/sty338
Fadda D., Girardi M., Giuricin G., Mardirossian F., Mezzetti M., 1996, ApJ, 473, 670. doi:10.1086/178180
Gunn J. E., Gott J. R., 1972, ApJ, 176, 1. doi:10.1086/151605
Pasquali A., Smith R., Gallazzi A., De Lucia G., Zibetti S., Hirschmann M., Yi S. K., 2019, MNRAS, 484, 1702. doi:10.1093/mnras/sty3530
Ribeiro A. L. B., Lopes P. A. A., Trevisan M., 2010, MNRAS, 409, L124. doi:10.1111/j.1745-3933.2010.00962.x
Rhee J., Smith R., Choi H., Yi S. K., Jaffé Y., Candlish G., Sánchez-Jánssen R., 2017, ApJ, 843, 128. doi:10.3847/1538-4357/aa6d6c
Ribeiro A. L. B., de Carvalho R. R., Trevisan M., Capelato H. V., La Barbera F., Lopes P. A. A., Schilling A. C., 2013, MNRAS, 434, 784. doi:10.1093/mnras/stt1071
Roberts I. D., Parker L. C., 2017, MNRAS, 467, 3268. doi:10.1093/mnras/stx317
Roberts I. D., Parker L. C., 2019, MNRAS, 490, 773. doi:10.1093/mnras/stz2666
Sampaio V. M., de Carvalho R. R., Ferreras I., Laganá T. F., Ribeiro A. L. B., Rembold S. B., 2021, MNRAS, 503, 3065. doi:10.1093/mnras/stab673
Sánchez-Blázquez P., Peletier R. F., Jiménez-Vicente J., Cardiel N., Cenarro A. J., Falcón-Barroso J., Gorgas J., et al., 2006, MNRAS, 371, 703. doi:10.1111/j.1365-2966.2006.10699.x
Schuecker P., Böhringer H., Reiprich T. H., Feretti L., 2001, A&A, 378, 408. doi:10.1051/0004-6361:20011215
de Vaucouleurs G., 1963, ApJS, 8, 31. doi:10.1086/190084
Yang X., Mo H. J., van den Bosch F. C., Jing Y. P., 2005, MNRAS, 356, 1293. doi:10.1111/j.1365-2966.2005.08560.x
Yang X., Mo H. J., van den Bosch F. C., Pasquali A., Li C., Barden M., 2007, ApJ, 671, 153. doi:10.1086/522027
Wetzel A. R., Tinker J. L., Conroy C., 2012, MNRAS, 424, 232. doi:10.1111/j.1365-2966.2012.21188.x